

Fall 10-11-2021

Diffusional fractionation of helium isotopes in silicate melts

Haiyang Luo
hluo5@lsu.edu

Bijaya Karki
Louisiana State University

Dipta B. Ghosh
Louisiana State University

Huiming Bao
Louisiana State University

Follow this and additional works at: https://digitalcommons.lsu.edu/geo_pubs



Part of the [Geochemistry Commons](#), and the [Geology Commons](#)

Recommended Citation

Luo, H., Karki, B., Ghosh, D., & Bao, H. (2021). Diffusional fractionation of helium isotopes in silicate melts. *Geochemical Perspectives Letters*, v19, 19-22. <https://doi.org/10.7185/geochemlet.2128>

This Article is brought to you for free and open access by the Department of Geology and Geophysics at LSU Digital Commons. It has been accepted for inclusion in Faculty Publications by an authorized administrator of LSU Digital Commons. For more information, please contact ir@lsu.edu.

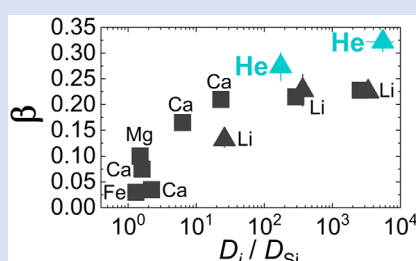
Diffusional fractionation of helium isotopes in silicate melts

H. Luo^{1*}, B.B. Karki^{1,2}, D.B. Ghosh², H. Bao¹



doi: 10.7185/geochemlet.2128

Abstract



Estimating Helium (He) concentration and isotope composition of the mantle requires quantifying He loss during magma degassing. The knowledge of diffusional He isotope fractionation in silicate melts may be essential to constrain the He loss. Isotopic mass dependence of He diffusion can be empirically expressed as $D^3\text{He}/D^4\text{He} = (4/3)^\beta$, where D is the diffusivity of a He isotope. However, no studies have reported any β values for He in silicate melts due to technical challenges in both experiments and computations. Here, molecular dynamics simulations based on deep neural network potentials trained by *ab initio* data show that β for He in albite melt decreases from 0.355 ± 0.012 at 3000 K to 0.322 ± 0.019 at 1700 K. β in model basalt melt takes a smaller value from 0.322 ± 0.025 to 0.274 ± 0.027 over the same temperature range. Based on our results, we suggest using $D^3\text{He}/D^4\text{He}$ values of 1.097 ± 0.006 and 1.082 ± 0.008 in natural rhyolite and basalt melt, respectively, to interpret measured He concentration and isotope composition of natural samples.

Received 26 April 2021 | Accepted 31 August 2021 | Published 13 October 2021

Letter

Noble gases are known to be chemically inert, which means that their compositions were not altered by chemical or biological processes over the Earth's history. Only physical processes such as diffusion, adsorption, or ion implantation may cause significant elemental and isotopic fractionations (Moreira, 2013). The inert behaviour combined with the existence of both radiogenic and non-radiogenic isotopes for each noble gas provides powerful tools for constraining mantle degassing history and identifying long lived heterogeneities within the mantle (Behrens, 2010; Moreira, 2013; Moreira and Kurz, 2013). However, measured noble gas isotope ratios in mid-ocean ridge basalts (MORB) and oceanic island basalts (OIB) are often difficult to interpret due to possible fractionations that happen in magma degassing (Moreira and Kurz, 2013).

Magma degassing occurs in a closed or open system. The changes of noble gas isotope compositions during closed system degassing are determined by equilibrium isotope fractionation between noble gases dissolved in the melt and noble gases in the gas phase. In comparison, magma degassing in an open system may be diffusion controlled (Watson, 2017) and diffusion can fractionate isotopes considerably even at magmatic temperatures (e.g., Richter et al., 1999; Watkins et al., 2017). Diffusional separation of isotopes can be expressed as (Richter et al., 1999):

$$\frac{D_i}{D_j} = \left(\frac{m_j}{m_i} \right)^\beta \quad \text{Eq. 1}$$

where D_i and D_j are diffusion coefficients of two isotopes whose masses are m_i and m_j and β is a dimensionless empirical parameter. The knowledge of β for noble gases in silicate melts is

essential to interpret noble gas isotope ratios. However, no experiments have studied diffusional fractionation of noble gas isotopes in high temperature silicate melts. The results from previous diffusion experiments using silicate glasses (Shelby, 1971; Trull and Kurz, 1999) may not be extrapolated to the cases in silicate melts, although silicate glasses are widely regarded as proper structural analogues of silicate melts. The reason is that the dynamics of silicate networks in high temperature melts help open and close paths for noble gas diffusion, which may play a key role in determining diffusional isotope fractionation (Behrens, 2010; Watkins et al., 2017). Additionally, it is known that the diffusivities of noble gases show non-Arrhenius behaviour around the glass transition temperature (Behrens, 2010; Amalberti et al., 2016), which may imply a change in diffusion mechanism and thus influence diffusional isotope fractionation.

First principles molecular dynamics (FPMD) simulations are reliable to calibrate β in liquids (Luo et al., 2020), but the high computational cost makes them unsuitable to deal with trace elements (e.g., noble gases and Li). A recently developed technique called deep potential molecular dynamics (DPMD) simulations (Wang et al., 2018; Zhang et al., 2018), which is based on potentials trained by deep neural networks using *ab initio* data and is orders of magnitude faster than FPMD with comparable *ab initio* accuracy, has been successfully applied to predict β for Li in silicate melts (Luo et al., 2021). Here we perform DPMD simulations to study diffusional He isotope fractionation in albite and model basalt melts at 3000, 2200, and 1700 K around zero pressure. The major technical improvement in this study is that the deep potential generator (DP-GEN) (Zhang et al., 2020) is used to achieve a concurrent learning procedure and to obtain a representative training data set in a rigorous way (Supplementary Information).

1. Department of Geology & Geophysics, Louisiana State University, Baton Rouge, LA 70803, USA

2. School of Electrical Engineering and Computer Science, Louisiana State University, Baton Rouge, LA 70803, USA

* Corresponding author (email: hluo5@lsu.edu)



Albite and model basalt melts (excess Ca to compensate Fe) are close analogues of natural rhyolite and basalt melts, respectively. One He atom is added to the albite melt containing $8\text{ NaAlSi}_3\text{O}_8$ (104 atoms) and the model basalt melt containing $\text{Ca}_9\text{Mg}_6\text{Al}_6\text{Si}_{18}\text{O}_{60}$ (99 atoms), respectively. We conduct the simulations at 3000 K for 1 nanosecond (ns) with a time step of 0.5 femtosecond (fs) and at 2200 and 1700 K for 4 ns with a time step of 1.0 fs. Each simulation is repeated five times with different initial configurations. The accuracy of DPMD simulations is validated by comparing the predicted energies (Fig. S-1), forces (Fig. S-2), and radial distribution functions (Fig. S-3) with those calculated from FPMD simulations. To derive a reliable β from the linear fitting of $\log D$ vs. $\log M$ based on Equation 1, we use two pseudo-isotopes with masses $M^* = 1$ and 2 g/mol, in addition to the two natural He isotopes (^3He and ^4He). The self diffusivities of the four He isotopes are calculated using the Einstein relation (Einstein, 1956):

$$D_{\text{He}} = \lim_{t \rightarrow \infty} \frac{\langle |\vec{r}(t + t_0) - \vec{r}(t_0)|^2 \rangle_{\text{He}}}{6t} \quad \text{Eq. 2}$$

where $\vec{r}(t)$ represents the particle trajectories and $\langle \dots \rangle_{\text{He}}$ denotes average mean square displacement (MSD) over time from different time origins t_0 . The average value over the five independent simulations and the corresponding confidence interval (± 2 s.e.) on the diffusivities are reported. The finite size effect on the diffusivities of He isotopes is insignificant within error after considering the correction relation proposed by Yeh and Hummer (Yeh and Hummer, 2004).

In Figure 1, linear MSD-time curves indicate that the diffusion of He isotopes was sampled well. All MSD curves for the four He isotopes at each condition are clearly separated. As suggested in previous studies (e.g., Bourg and Sposito, 2007; Luo *et al.*, 2020), only the first part of MSD curves in the diffusive regime (9–10 picoseconds (ps), 20–40 ps, and 50–100 ps at 3000, 2200, and 1700 K, respectively) is used to approximate the infinite time limit in Equation 2. We find that He diffuses much faster in albite than in model basalt melts, consistent with the trend found in glasses (Behrens, 2010). Calculated diffusion coefficients of He isotopes display a negative correlation with mass and a positive correlation with temperature

in both albite and model basalt melts (Table S-1, Fig. 2a). The temperature dependence of diffusivities is fit to the Arrhenius relation:

$$D_{\alpha} = D_{0\alpha} \exp \left[\frac{-E_{\alpha}}{RT} \right] \quad \text{Eq. 3}$$

where α represents a He isotope. The predicted pre-exponential factor ($D_{0\alpha}$) and activation energy (E_{α}) appear to decrease with increasing isotopic mass of He (Fig. S-4). The predicted diffusivity for ^4He in model basalt melt at 1623 K is $4.81 \times 10^{-9} \text{ m}^2/\text{s}$, which agrees well with the experimental value of $5 \times 10^{-9} \text{ m}^2/\text{s}$ in a tholeiitic melt (Lux, 1987) and the computational result from classical MD in a MORB melt (Guillot and Sator, 2012), although it is unclear why an experiment reported a much lower value of $0.28 \times 10^{-9} \text{ m}^2/\text{s}$ in model basalt melt at 1673 K (Amalberti *et al.*, 2018). E_{α} for ^4He in albite and model basalt melts are 27.9 ± 7.6 and 65.8 ± 2.4 kJ/mol, respectively. No experiments have reported activation energy for He diffusion in silicate melts. The experimental activation energies for He diffusion in albite and basalt glasses at much lower temperatures (398–673 K) are 31.7 (Shelby and Eagan, 1976) and 83 ± 4 kJ/mol (Kurz and Jenkins, 1981), respectively. The smaller activation energies predicted by FPMD simulations compared to experimental results have been extensively reported (Karki *et al.*, 2018). The very different temperature ranges explored in simulations and experiments may account for the discrepancy. It is worth stressing that He diffusion in albite melt shows a small non-Arrhenius behaviour (Fig. 2a).

The linear correlation of $\log D$ with $\log M$ in Figure 2b is consistent with the empirical Equation 1 proposed by Richter *et al.* (1999). The calculated β in albite melt decreases from 0.355 ± 0.012 at 3000 K to 0.322 ± 0.019 at 1700 K. In comparison, β in model basalt melt takes a smaller value from 0.322 ± 0.025 to 0.274 ± 0.027 over the same temperature range. The smaller β value in model basalt than in albite melt is the same as that observed in the case of Li, which makes sense as both He and Li diffuse faster in rhyolitic than in basaltic melt due to higher ionic porosity of rhyolitic melt. The decreasing trend of β with temperature in silicate melts around zero pressure has been reported in the simulations of diffusional Mg and Li isotope fractionation (Luo *et al.*, 2020, 2021). An assumed linear regression fit to β vs. T^{-1} yields relationships: $\beta = (0.397 \pm 0.017)$

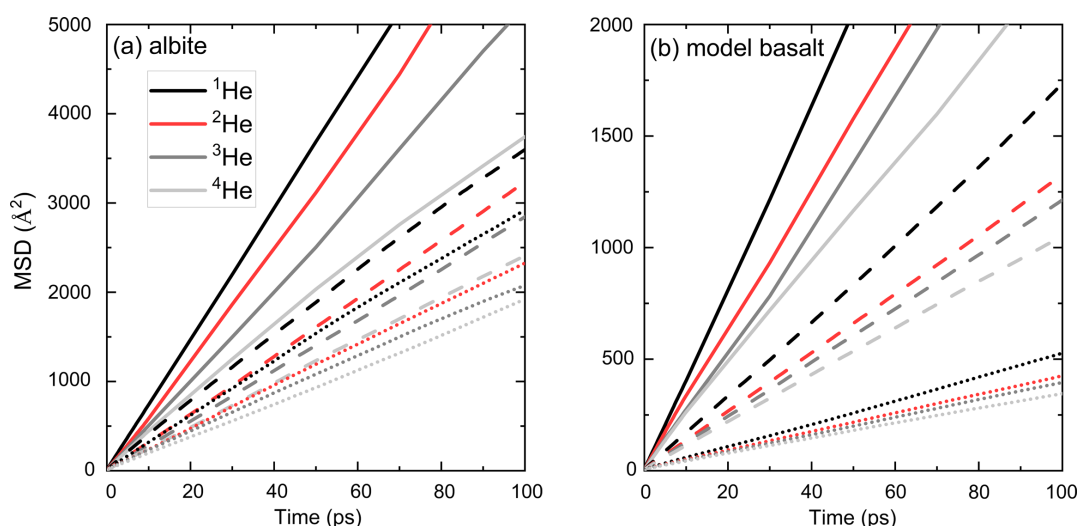


Figure 1 Mean square displacement (MSD) of He isotopes (^1He , ^2He , ^3He , ^4He) as a function of time in (a) albite and (b) model basalt melts at 3000 (solid lines), 2200 (dashed lines), and 1700 K (dotted lines) around zero pressure.

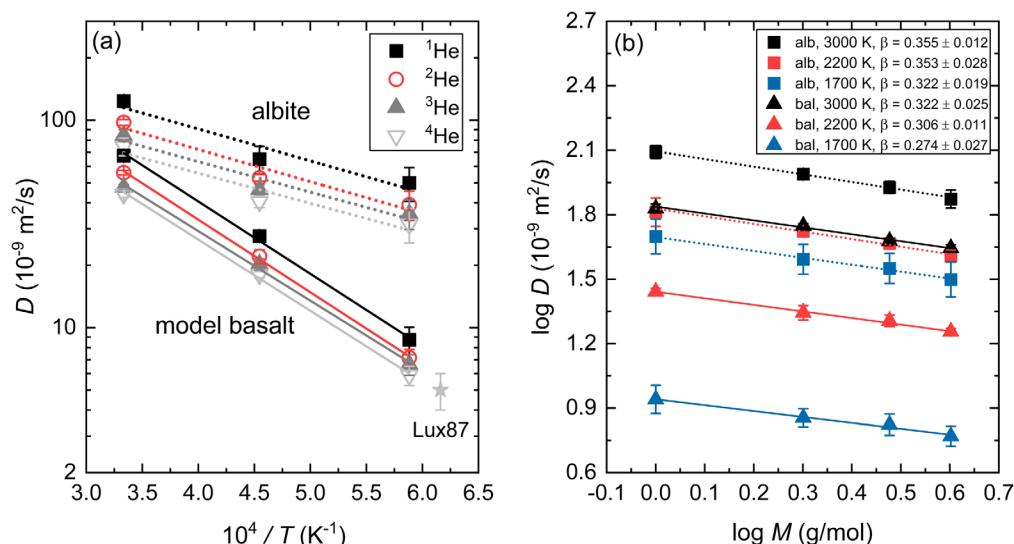


Figure 2 (a) Diffusion coefficients of He isotopes (^1He , ^2He , ^3He , ^4He) as a function of temperature in albite and model basalt melts around zero pressure. The experimental data (Lux87) for the diffusivity of He in a tholeiitic melt is from Lux (1987). (b) Log-log plot of the diffusivities of He isotopes in albite (alb) and model basalt (bal) melts as a function of isotopic mass at different temperatures around zero pressure.

$-(0.012 \pm 0.004) \times 10^4/T$ in albite melt and $\beta = (0.389 \pm 0.021) - (0.019 \pm 0.005) \times 10^4/T$ in model basalt melt. The stronger temperature dependence of β for Li in model basalt than in albite melt is also observed here for He. Based on the predicted β values, a drop of temperature by 300 K (1700–1400 K in basaltic melt or 1400–1100 K in rhyolitic melt) results in a negligible decrease ($\sim 0.7\%$) of $D^3\text{He}/D^4\text{He}$ value. Thus, we suggest that using the data at 1700 K, $D^3\text{He}/D^4\text{He}$ values of 1.082 ± 0.008 in model basalt melt and 1.097 ± 0.006 in albite melt, are accurate enough when dealing with diffusional fractionation of He isotopes in natural silicate melts at shallow depths of the present day Earth.

It has been proposed that β positively correlates with solvent normalised diffusivity (D_i/D_{Si}), implying that cations that are easier to decouple from the silicate matrix exhibit a larger diffusional isotope fractionation (Watkins *et al.*, 2011, 2017). Note

that Luo *et al.* (2020, 2021) stressed that this positive correlation only works at a constant or narrowly defined temperature range as β in silicate melts is found to decrease with decreasing temperature while D_i/D_{Si} increases. The correlation of β for He with $D_{\text{He}}/D_{\text{Si}}$ at 1700 K broadly follows the previous positive trend (Fig. 3). The value of $D_{\text{He}}/D_{\text{Si}}$ is $\sim 5525 \pm 2378$ in albite melt, much larger than the value of $\sim 174 \pm 37$ in model basalt melt. However, it seems that the overall relationship between β and D_i/D_{Si} becomes less defined even at a narrow temperature range when data for different elements in different melt systems are considered (Fig. 3). This could be attributed to different extents of compositional dependence of both β and D_i/D_{Si} . More data are needed to further explore this issue.

Helium is the fastest diffusing species in natural silicate melts (except H_2 which is easily oxidised) and there is a positive correlation between diffusivity and β at fixed temperatures. Thus, it is fair to say that the overall range of β for different elements in natural silicate melts is ~ 0 – 0.32 . The largest β value is given by He isotope diffusion in rhyolitic melt, which is still much lower

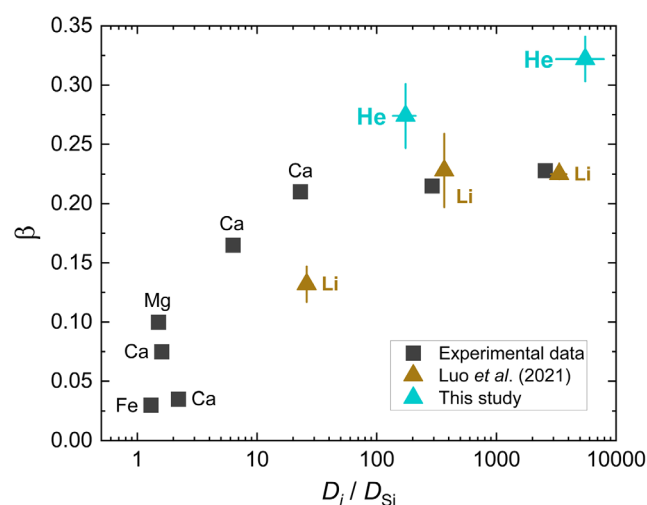


Figure 3 Relationship of β with solvent normalised diffusivity (D_i/D_{Si}). Experimental data is from Richter *et al.* (2003, 2009), Watkins *et al.* (2009, 2011), and Holycross *et al.* (2018). Computational results of Li at 1800 K are from Luo *et al.* (2021). All data shown here are for the relatively narrow temperature range 1623–1800 K, except one data point from Holycross *et al.* (2018).

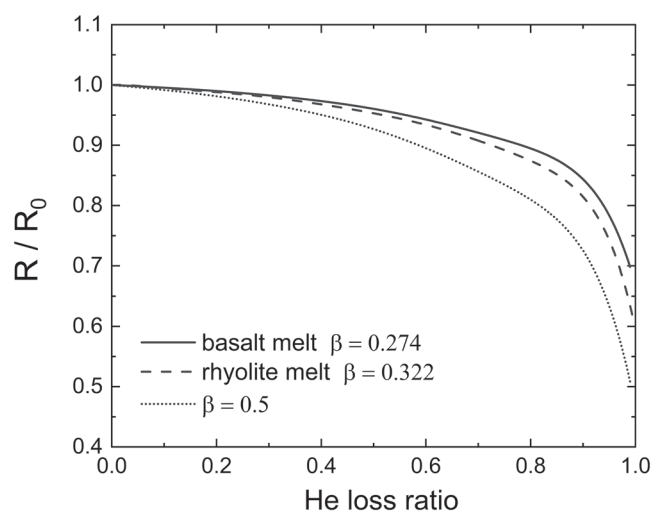


Figure 4 $(^3\text{He}/^4\text{He})/(^3\text{He}/^4\text{He})_0$ as a function of He loss ratio for different β values.

than the value of 0.5 in the case of ideal gas. Given measured He isotope ratios of geological samples (rocks, minerals, glasses, or melt inclusions) that went through diffusive degassing at the magmatic stage, a smaller β value means that the samples must have lost more He than previously thought.

For example, reducing an initial $^3\text{He}/^4\text{He}$ ratio by 10 % requires 60 % gas loss for β equal to 0.5, but 73 % loss for β of 0.322 in rhyolite melt and 77 % loss for β of 0.274 in basalt melt (Fig. 4, Supplementary Information). Our reported β values are useful for quantitatively estimating He loss during magmatic degassing and trace back He concentration and isotope composition of magma source region.

Acknowledgements

The research is supported by the Strategic Priority Research Program (B) of Chinese Academy of Sciences (XDB18010104) and National Science Foundation (EAR 1764140 and 2001074). High-performance computing resources were provided by Louisiana State University.

Editor: Anat Shahar

Additional Information

Supplementary Information accompanies this letter at <https://www.geochemicalperspectivesletters.org/article2128>.



© 2021 The Authors. This work is distributed under the Creative Commons Attribution Non-Commercial No-Derivatives 4.0

License, which permits unrestricted distribution provided the original author and source are credited. The material may not be adapted (remixed, transformed or built upon) or used for commercial purposes without written permission from the author. Additional information is available at <https://www.geochemicalperspectivesletters.org/copyright-and-permissions>.

Cite this letter as: Luo, H., Karki, B.B., Ghosh, D.B., Bao, H. (2021) Diffusional fractionation of helium isotopes in silicate melts. *Geochem. Persp. Let.* 19, 19–22.

References

- AMALBERTI, J., BURNARD, P., LAPORTE, D., TISSANDIER, L., NEUVILLE, D.R. (2016) Multidiffusion mechanisms for noble gases (He, Ne, Ar) in silicate glasses and melts in the transition temperature domain: Implications for glass polymerization. *Geochimica et Cosmochimica Acta* 172, 107–126.
- AMALBERTI, J., BURNARD, P., TISSANDIER, L., LAPORTE, D. (2018) The diffusion coefficients of noble gases (He–Ar) in a synthetic basaltic liquid: One-dimensional diffusion experiments. *Chemical Geology* 480, 35–43.
- BEHRENS, H. (2010) Noble Gas Diffusion in Silicate Glasses and Melts. *Reviews in Mineralogy and Geochemistry* 72, 227–267.
- BOURG, I.C., SPOSITO, G. (2007) Molecular dynamics simulations of kinetic isotope fractionation during the diffusion of ionic species in liquid water. *Geochimica et Cosmochimica Acta* 71, 5583–5589.
- EINSTEIN, A. (1956) *Investigations on the Theory of Brownian Movement*. First Edition, Dover, New York.
- GUILLLOT, B., SATOR, N. (2012) Noble gases in high-pressure silicate liquids: A computer simulation study. *Geochimica et Cosmochimica Acta* 80, 51–69.
- HOLYCROSS, M.E., WATSON, E.B., RICHTER, F.M., VILLENEUVE, J. (2018) Diffusive fractionation of Li isotopes in wet, highly silicic melts. *Geochemical Perspectives Letters* 6, 39–42.
- KARKI, B.B., GHOSH, D.B., BAIGAIN, S.K. (2018) Chapter 16 - Simulation of Silicate Melts Under Pressure. In: KONO, Y., SANLOUP, C. (Eds.) *Magnas Under Pressure*. First Edition, Elsevier, Amsterdam, 419–453.

- KURZ, M.D., JENKINS, W.J. (1981) The distribution of Helium in oceanic basalt glasses. *Earth and Planetary Science Letters* 53, 41–54.
- LUO, H., KARKI, B.B., GHOSH, D.B., BAO, H. (2020) First-principles computation of diffusional Mg isotope fractionation in silicate melts. *Geochimica et Cosmochimica Acta* 290, 27–40.
- LUO, H., KARKI, B.B., GHOSH, D.B., BAO, H. (2021) Deep neural network potentials for diffusional lithium isotope fractionation in silicate melts. *Geochimica et Cosmochimica Acta* 303, 38–50.
- LUX, G. (1987) The behavior of noble gases in silicate liquids-solution, diffusion, bubbles and surface effects, with applications to natural samples. *Geochimica et Cosmochimica Acta* 51, 1549–1560.
- MOREIRA, M. (2013) Noble Gas Constraints on the Origin and Evolution of Earth's Volatiles. *Geochemical Perspectives* 2, 229–230.
- MOREIRA, M.A., KURZ, M.D. (2013) Noble Gases as Tracers of Mantle Processes and Magmatic Degassing. In: BURNARD, P. (Ed.) *The Noble Gases as Geochemical Tracers. Advances in Isotope Geochemistry*. First Edition, Springer-Verlag, Berlin, Heidelberg, 371–391.
- RICHTER, F.M., LIANG, Y., DAVIS, A.M. (1999) Isotope fractionation by diffusion in molten oxides. *Geochimica et Cosmochimica Acta* 63, 2853–2861.
- RICHTER, F.M., DAVIS, A.M., DEPAOLO, D.J., WATSON, E.B. (2003) Isotope fractionation by chemical diffusion between molten basalt and rhyolite. *Geochimica et Cosmochimica Acta* 67, 3905–3923.
- RICHTER, F.M., WATSON, E.B., MENDYBAEV, R., DAUPHAS, N., GEORG, B., WATKINS, J., VALLEY, J. (2009) Isotopic fractionation of the major elements of molten basalt by chemical and thermal diffusion. *Geochimica et Cosmochimica Acta* 73, 4250–4263.
- SHELBY, J.E. (1971) Diffusion of Helium isotopes in vitreous silica. *Physical Review B* 4, 2681–2686.
- SHELBY, J.E., EAGAN, R.J. (1976) Helium migration in sodium aluminosilicate glasses. *Journal of the American Ceramic Society* 59, 420–425.
- TRULL, T.W., KURZ, M.D. (1999) Isotopic fractionation accompanying helium diffusion in basaltic glass. *Journal of Molecular Structure* 485, 555–567.
- WANG, H., ZHANG, L.F., HAN, J.Q., E, W. (2018) DeePMD-kit: A deep learning package for many-body potential energy representation and molecular dynamics. *Computer Physics Communications* 228, 178–184.
- WATKINS, J.M., DEPAOLO, D.J., HUBER, C., RYERSON, F.J. (2009) Liquid composition-dependence of calcium isotope fractionation during diffusion in molten silicates. *Geochimica et Cosmochimica Acta* 73, 7341–7359.
- WATKINS, J.M., DEPAOLO, D.J., RYERSON, F.J., PETERSON, B.T. (2011) Influence of liquid structure on diffusive isotope separation in molten silicates and aqueous solutions. *Geochimica et Cosmochimica Acta* 75, 3103–3118.
- WATKINS, J.M., DEPAOLO, D.J., WATSON, E.B. (2017) Kinetic Fractionation of Non-Traditional Stable Isotopes by Diffusion and Crystal Growth Reactions. *Non-Traditional Stable Isotopes* 82, 85–125.
- WATSON, E.B. (2017) Diffusive fractionation of volatiles and their isotopes during bubble growth in magmas. *Contributions to Mineralogy and Petrology* 172, 61.
- YEH, I.-C., HUMMER, G. (2004) System-Size Dependence of Diffusion Coefficients and Viscosities from Molecular Dynamics Simulations with Periodic Boundary Conditions. *The Journal of Physical Chemistry B* 108, 15873–15879.
- ZHANG, L.F., HAN, J.Q., WANG, H., SAIDI, W., CAR, R., E, W. (2018) End-to-end symmetry preserving inter-atomic potential energy model for finite and extended systems. *Advances of the Neural Information Processing Systems* 31, 4441–4451.
- ZHANG, Y.Z., WANG, H.D., CHEN, W.J., ZENG, J.Z., ZHANG, L.F., WANG, H., E, W. (2020) DP-GEN: A concurrent learning platform for the generation of reliable deep learning based potential energy models. *Computer Physics Communications* 253, 107206.



Diffusional fractionation of helium isotopes in silicate melts

H. Luo, B.B. Karki, D.B. Ghosh, H. Bao

Supplementary Information

The Supplementary Information includes:

- Deep Potential Training
- Numerical Modelling of Diffusion
- Table S-1
- Figures S-1 to S-4
- Supplementary Information References

Deep Potential Training

We constructed the deep-learning potential (DP) models for helium-bearing albite and model basalt melt using the DP-GEN (Zhang *et al.*, 2020) scheme for the configurational space covering a temperature range 1400–4000 K and a volume range 1.0–1.1 V_a ($V_a = 1435 \text{ \AA}^3$) for helium-bearing albite melt and 0.89–1.09 V_b ($V_b = 1389 \text{ \AA}^3$) for helium-bearing model basalt melt. The DP-GEN scheme works iteratively, and each iteration includes three stages, exploration, labeling, and training. To begin with, rough DP models are first trained by a simple data set. The following are the details of our training setups.

Initial data set. We randomly picked 10 configurations (1 He + 8 NaAlSi₃O₈, 105 atoms for helium-bearing albite melt and 1 He + Ca₉Mg₆Al₆Si₁₈O₆₀, 100 atoms for helium-bearing model basalt melt) at each volume (1.0 V_a , 1.02 V_a , 1.05 V_a , and 1.1 V_a , where $V_a = 1435 \text{ \AA}^3$ for helium-bearing albite melt and 0.89 V_b , 0.94 V_b , 1.0 V_b , and 1.09 V_b , where $V_b = 1389 \text{ \AA}^3$ for helium-bearing model basalt melt) from first-principles molecular dynamics (FPMD) simulations as the initial configurations. Then short-time (40 femtoseconds) and high-precision (see the labeling step) FPMD simulations starting from each of the initial configurations were performed to generate the initial data set, which were labeled with energy and force.

Exploration. DP-based molecular dynamics (DPMD) simulations using the LAMMPS package (Plimpton, 1995) interfaced with the DeepMD-kit (Wang *et al.*, 2018) were performed to explore the configurational space. In each

iteration, canonical (NVT) simulations of 4 volumes as used in creating the initial data set and 6 temperatures (1400, 1700, 2200, 3000, 3500, 4000 K) were conducted. The time duration of these simulations increased from 1 to 10 picosecond (ps) with increasing iterations (*i.e.*, 1 ps in the first iteration, 3 ps in the second iteration, 6 ps in the third iteration, 10 ps in the fourth and remaining iterations until convergence). The explored configurations are categorized as failed, candidate, and accurate, according to the maximum deviation of forces (δ_f^{max}), defined as $\delta_f^{max} = \max_i \sqrt{\langle \|f_i - \langle f_i \rangle\|^2 \rangle}$, where f_i is the force acting on atom i , and $\langle \dots \rangle$ represents the average of the DP model ensemble. The failed and accurate sets include configurations with large force deviations ($\delta_f^{max} > \delta_{high}$) and small force deviations ($\delta_f^{max} < \delta_{low}$), respectively, where δ_{high} and δ_{low} are user-provided. The configurations with maximum force deviations between δ_{low} and δ_{high} are classified as candidates. A good convergence of the DP-GEN iterations is achieved when almost all the explored configurations are categorized as accurate. The lower and higher force deviations (δ_{low} and δ_{high}) were set to be 0.15 and 0.40 eV/Å for the first 8 iterations, 0.25 and 0.50 eV/Å for the second 6 iterations. In each iteration, 300 configurations in the candidate set were randomly picked and sent to the labelling stage.

Labelling. DFT calculations were conducted within local density approximation (Ceperley and Alder, 1980) and projector augmented wave method (Blochl, 1994; Kresse and Joubert, 1999) using Vienna Ab-initio Simulation package (Kresse and Furthmüller, 1996). We used a plane-wave cutoff energy of 700 eV and Gamma-point Brillouin-zone sampling. The convergence criterion of the self-consistent field (SCF) was set to be 10^{-6} eV.

Training. The smoothed version of DP (Zhang *et al.*, 2018) implemented in DeepMD-kit (1.2.0) (Wang *et al.*, 2018) was applied to train the potential energy surface. The sizes of the embedding and fitting networks were set to be (25, 50, 100) and (240, 240, 240). The radial cutoff was chosen to be 6.0 Å in the DP-GEN iterations. The start learning rate, decay rate, and decay steps were 0.001, 0.95, and 2000, respectively. In each iteration, four DP models were trained for 400, 000 steps with the same architecture and data set but different initial model parameters. After the DP-GEN iterations were converged, we generated the final DP model with a radial cutoff set to 7.0 Å and training steps set to 1,000,000 with the decay step set to 5000. A new exploration stage begins by using the newly trained DP models based on the updated data set.

In total, we performed 14 DP-GEN iterations and about 2.88 million helium-bearing albite melt configurations were explored, so as for helium-bearing model basalt melt. A small portion (~0.15 %) of them was selected for labeling. The percentage of configurations categorized as accurate in the exploration stage of the last iteration was around 99 %. With two well-trained DP models for the two melts, respectively, we first equilibrated the systems in the NPT ensemble at different temperatures (3000, 2200, 1700 K) and zero pressure to extract the corresponding cell volumes. Then we performed canonical (NVT) simulations for each He isotope. The volumes we obtained are $V_a = 1570, 1535, \text{ and } 1505 \text{ Å}^3$ at 3000, 2200, and 1700 K, respectively; $V_b = 1390, 1338, \text{ and } 1300 \text{ Å}^3$ at 3000, 2200, and 1700 K, respectively.



Numerical Modelling of Diffusion

The evolution of He concentration profile in melts during diffusive gas loss can be described by:

$$\frac{\partial C}{\partial t} = D \frac{\partial^2 C}{\partial x^2},$$

where the initial concentration distribution is $C = C_0$ for all values of x and one boundary concentration distribution is $\partial C(x = 0, t > 0)/\partial x = 0$. Diffusivities of He in rhyolite and basalt melt at 1100 and 1400 K, respectively, are estimated by using our fitted Arrhenius relationship. Experimental and thermodynamic constraints on He elemental/isotopic systematics during magma degassing is largely absent. Here we assume that the He concentration in the vapour at the melt-vapour interface, $C(x = L, t > 0)$, is zero. This simplification may make sense as He is highly volatile and in the vapour He diffuses several orders of magnitude faster than that in the melt. A non-zero He concentration in the vapour at the melt-vapour interface affects the absolute values of model predictions but not the overall conclusions as shown in Figure 4. The evolution of $(^3\text{He}/^4\text{He})/(^3\text{He}/^4\text{He})_0$ and He loss ratio are calculated by adding up all the corresponding values in the melt. Our results for β equal to 0.5 are close to the one calculated for spherical geometry (Trull and Kurz, 1999), suggesting that the geometry does not affect the overall conclusions either.



Supplementary Tables

Table S-1 Diffusion coefficients of He isotopes in albite and model basalt melts at different temperatures around zero pressure. Estimated diffusivities of ^4He in albite and model basalt melts at 3000 K from 100 ps FPMD simulations are $(69.8 \pm 12.3) \times 10^{-9}$ and $(41.6 \pm 5.6) \times 10^{-9} \text{ m}^2/\text{s}$, respectively.

	T (K)	M _{He} (g/mol)	D _{He} ($10^{-9} \text{ m}^2/\text{s}$)
albite	3000	1	124 ± 8
	3000	2	97.5 ± 3.2
	3000	3	84.6 ± 5.5
	3000	4	74.7 ± 7.2
	2200	1	64.9 ± 9.9
	2200	2	52.8 ± 1.9
	2200	3	46.4 ± 2.5
	2200	4	40.5 ± 2.6
	1700	1	49.9 ± 9.3
	1700	2	39.2 ± 6.3
	1700	3	35.5 ± 5.7
	1700	4	31.5 ± 5.9
model basalt	3000	1	67.5 ± 3.2
	3000	2	56.0 ± 1.6
	3000	3	47.6 ± 1.5
	3000	4	44.1 ± 1.7
	2200	1	27.6 ± 1.0
	2200	2	22.1 ± 1.7
	2200	3	20.2 ± 1.3
	2200	4	18.0 ± 0.6
	1700	1	8.72 ± 1.32
	1700	2	7.16 ± 0.69
	1700	3	6.65 ± 0.76
	1700	4	5.88 ± 0.63



Supplementary Figures

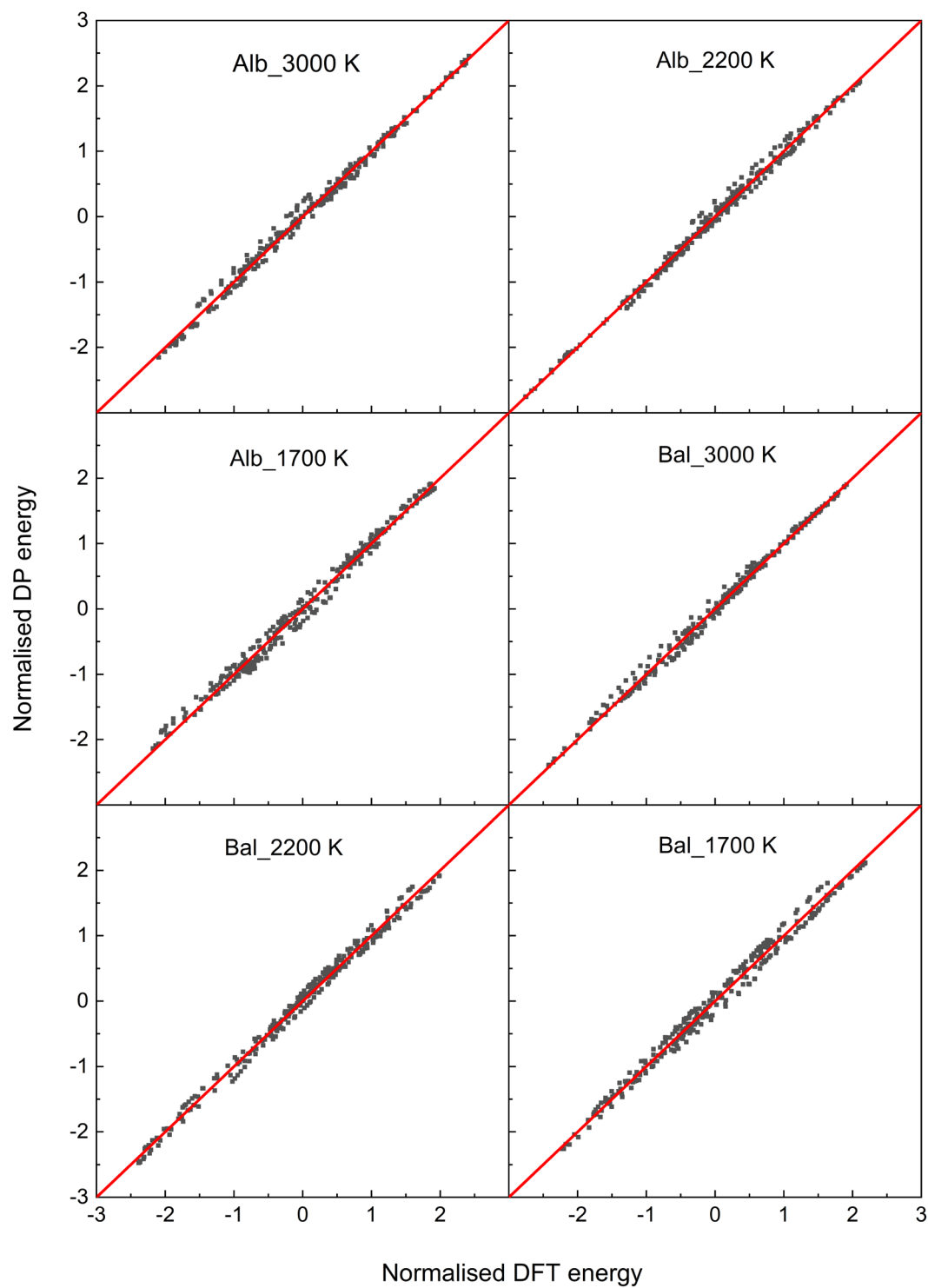


Figure S-1 Comparison of normalised energies calculated by deep potential (dp) and density functional theory (DFT) using a test data set.

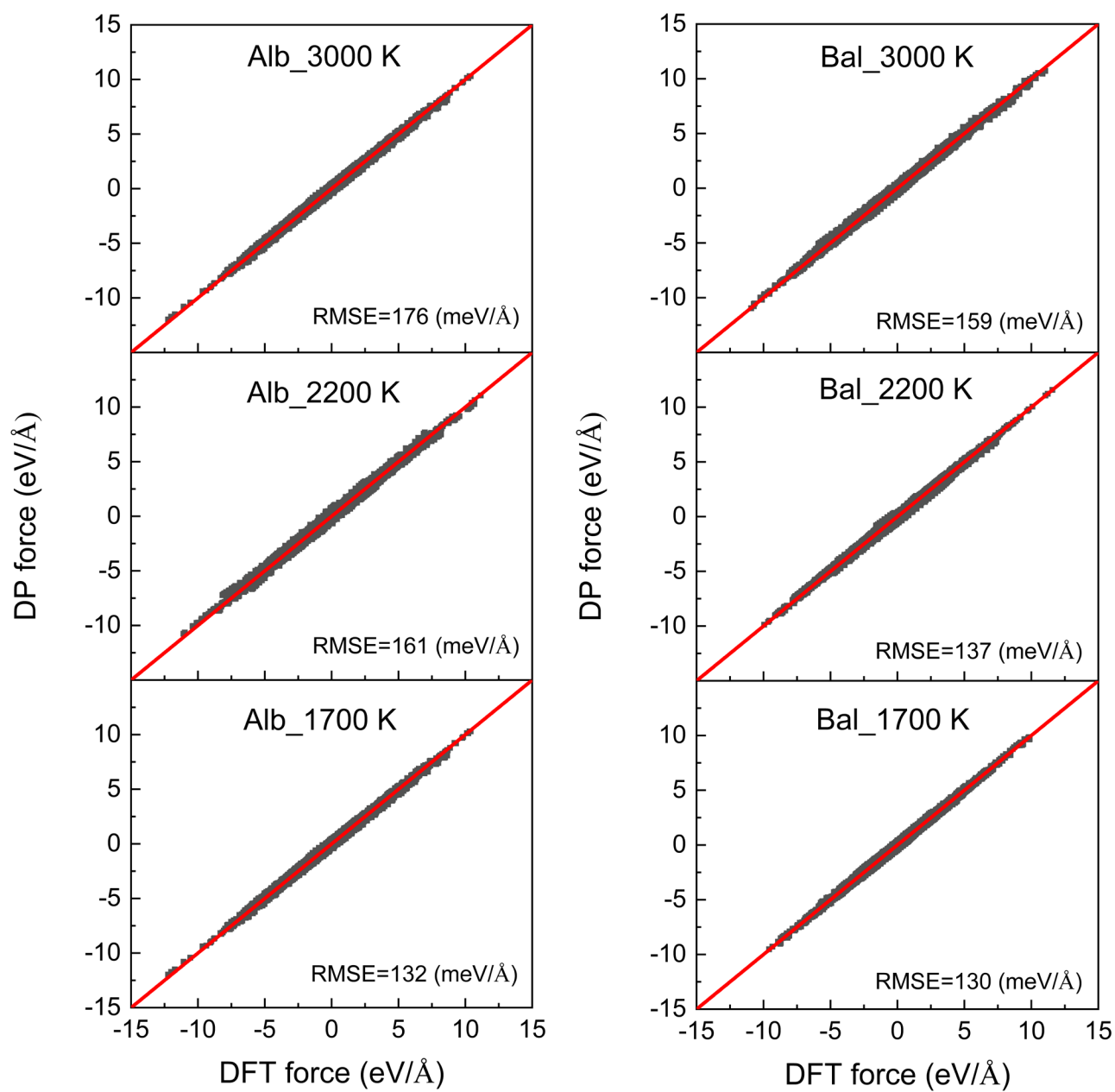


Figure S-2
data set.

Comparison of forces calculated by deep potential (dp) and density functional theory (DFT) using a test

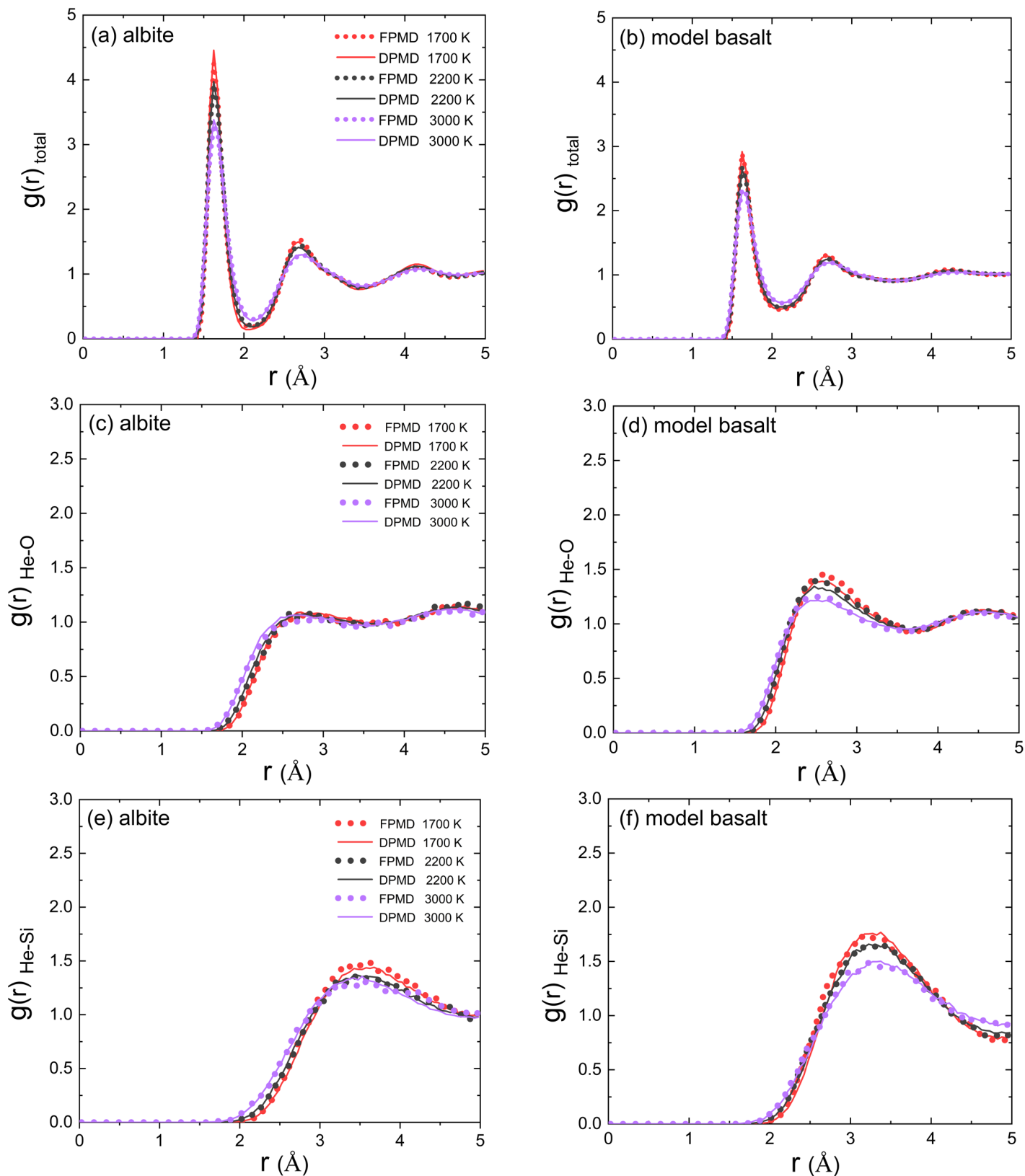


Figure S-3 Comparison of total (a and b) and partial (c-f) radial distribution functions calculated from DPMD and FPMD simulations. The FPMD data is more scattered due to limited sampling (50–150 ps).



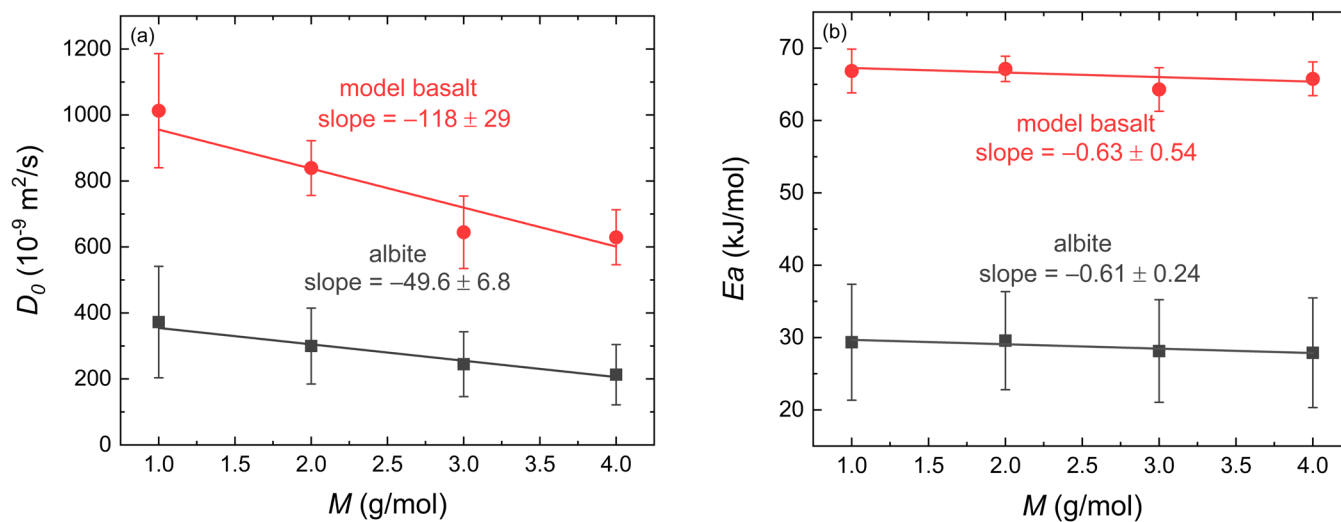


Figure S-4 The predicted pre-exponential factor ($D_{0\alpha}$) and activation energy (E_α) of He isotopes as a function of isotopic mass in albite and model basalt melts.

Supplementary Information References

- Bloch, P.E. (1994) Projector Augmented-Wave Method. *Physical Review B* 50, 17953-17979.
- Ceperley, D.M., Alder, B.J. (1980) Ground-State of the Electron-Gas by a Stochastic Method. *Physical Review Letters* 45, 566-569.
- Kresse, G., Furthmüller, J. (1996) Efficiency of ab-initio total energy calculations for metals and semiconductors using a plane-wave basis set. *Computational Materials Science* 6, 15-50.
- Kresse, G., Joubert, D. (1999) From ultrasoft pseudopotentials to the projector augmented-wave method. *Physical Review B* 59, 1758-1775.
- Plimpton, S. (1995) Fast Parallel Algorithms for Short-Range Molecular Dynamics. *Journal of Computational Physics* 117, 1-19.
- Trull, T.W., Kurz, M.D. (1999) Isotopic fractionation accompanying helium diffusion in basaltic glass. *Journal of Molecular Structure* 485, 555-567.
- Wang, H., Zhang, L.F., Han, J.Q., E, W.N. (2018) DeePMD-kit: A deep learning package for many-body potential energy representation and molecular dynamics. *Computer Physics Communications* 228, 178-184.
- Zhang, L.F., Han, J.Q., Wang, H., Saidi, W., Car, R., E, W. (2018) End-to-end symmetry preserving inter-atomic potential energy model for finite and extended systems. *Advances of the Neural Information Processing Systems*, 4441-4451.
- Zhang, Y.Z., Wang, H.D., Chen, W.J., Zeng, J.Z., Zhang, L.F., Wang, H., E, W. (2020) DP-GEN: A concurrent learning platform for the generation of reliable deep learning based potential energy models. *Computer Physics Communications* 253.

